PROCEEDINGS OF SCIENCE

# Galactic cosmic ray variations associated with February 2022 "Starlink" magnetic storms observed with global networks of neutron monitors and muon detectors

**Y. Masuda,**[a,*] **C. Kato,**[a] **Y. Hayashi,**[a] **M. Kozai,**[b] **R. Kataoka,**[c,d] **A. Kadokura,**[b,c,d] **S. Miyake,**[e] **K. Iwai**[f] **and K. Munakata**[a] **for the GMDN collaboration**

[a] *Department of Physics, Shinshu University, Matsumoto, Nagano 390-8621, Japan.*

[b] *Polar Environment Data Science Center, Joint Support-Center for Data Science Research, Research Organization of Information and Systems, Tachikawa, Tokyo 190-0014, Japan.*

[c] *National Institute of Polar Research, Tachikawa, Tokyo 190-8518, Japan.*

[d] *Department of Polar Science, School of Multidisciplinary Sciences, The Graduate University for Advanced Studies, SOKENDAI, Tachikawa, Tokyo 190-8518, Japan.*

[e] *National Institute of Technology (KOSEN), Ibaraki College,866 Nakane, Hitachinaka-shi, Ibaraki-ken 312-8508 Japan.*

[f] *Institute for Space-Earth Environmental Research, Nagoya University, Nagoya, Aichi 464-8601, Japan.*

*E-mail:* 23ss209d@shinshu-u.ac.jp

A bunch of Starlink satellites was launched after the peak of the first magnetic storm at 18:13 (UT) on February 3, and 38 of the 49 satellites re-entered the atmosphere during the succeeding second moderate magnetic storms. A global network of the ground-based multidirectional muon detectors, the Global Muon Detector Network (GMDN), has been continuously monitoring the intensity of cosmic rays arriving at Earth. Neutron monitors (NMs) are also monitoring cosmic ray variations in different energy ranges. In this paper, we analyze the cosmic ray decreases associated with the interplanetary shock and coronal mass ejections (ICMEs) which caused the sequence of "Starlink" magnetic storms observed with GMDN and NMs.

38th International Cosmic Ray Conference (ICRC2023)
26 July - 3 August, 2023
Nagoya, Japan

*Speaker





PoS(ICRC2023)1344

## 1. Introduction

Galactic cosmic ray (GCR) flux transiently varies with the solar storm. Ground-based cosmic ray observations, specifically observations in global network, provide us the information about GCR density and anisotropy during those storms hitting the Earth. This information helps us to understand various space weather events.

On February 3, 2022, there was an incident that Starlink satellites of SpaceX re-entered the aerospace after their launch. This incident is caused by unexpected second disturbances in the Earth's magnetic field [1]. Kataoka et al.(2022)[1] suggested the possibility from solar wind parameters that there were two flux ropes. A schematic view of their model and reference data (magnetic field, solar wind, and Dst-index) are shown in Figure 1 and 2, respectively. As shown in Figure 2, Kataoka et al.(2022) defined the shock-sheath (blue shaded), the first flux rope (FR1; yellow shaded), and the second flux rope (FR2; orange shaded) periods[1]. We analyze neutron monitor (NM) network and Global Muon Detector Network (GMDN) data recorded during this event to study variations in cosmic ray density and anisotropies. We report the preliminary results of the analysis.

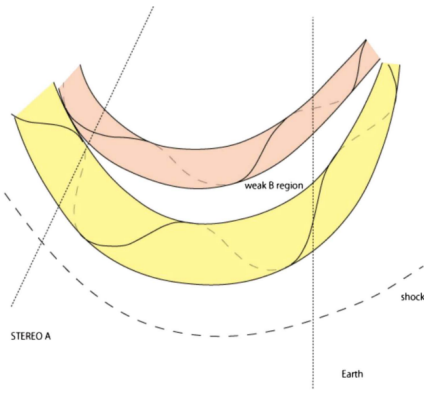


**Figure 1: Schematic illustration of two flux ropes encountering the Earth by [1]**

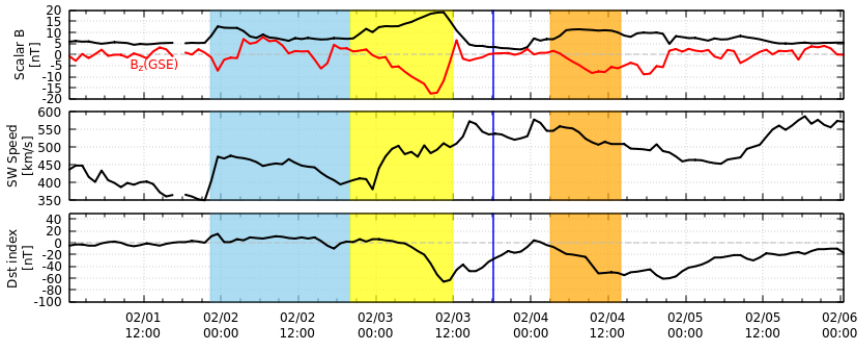


**Figure 2: Magnetic field data and solar wind data.**
From top to bottom, each panel displays the magnitude of the interplanetary magnetic field, the solar wind speed, and the Dst index. The GSE-$z$ component of the magnetic field is indicated by red curves in the top panel. Blue, yellow, and orange shaded periods indicate the shock-sheath, FR1, and FR2 periods defined by [1], respectively. The vertical blue lines in all panels indicate the launch time of Starlink satellites.

## 2. Data and Analysis

The GCR density and anisotropy are obtained by using hourly count rates observed by the NM network and the GMDN. Cosmic ray intensity variations in different rigidity regions can be monitored with the NM network and the GMDN. A cosmic ray density, first-order anisotropy, and second-order anisotropy are obtained separately, each as a function of time and the rigidity of primary cosmic rays, by fitting a model function to each of the observed count rates.

### 2.1 Cosmic ray data

We analyze hourly count rates recorded during 27 days between 22:00 (UT) on January 19 and 21:00 (UT) on February 15. They are 89 hourly count rates recorded by 20 NMs and 69 directional channels of the GMDN (hereafter MDs) and available on websites (NMDB : http://www01.nmdb.eu/, PSNM : http://www.thaispaceweather.com/, GMDN : https://cosray.shinshu-u.ac.jp/crest/DB/Documents/documents.php, see also [2]). The NM cosmic ray data available from these websites are all corrected for atmospheric pressure. The MD data are corrected not only for the atmospheric pressure but also for the atmospheric temperature effect by applying the method developed by [3]. This method uses the mass-weighted temperature calculated from the vertical profile of the atmospheric temperature provided by the Global Data Assimilation System (GDAS) of the National Center for Environmental Prediction (http://www.ready.noaa.gov). Table 1 lists NMs and MDs used in this paper with their characteristics. Our calculations of the median primary rigidity $P_m$, latitude and longitude of the asymptotic viewing direction ($\lambda_{asymp}$ and $\phi_{asymp}$), and the response functions used in our calculations are described in [4]. These 20 NMs are selected to maximize the range of viewing directions with less overlapping directions.

We particularly include the data from the PSNM (Princess Sirindhorn NM in Thailand) in operation at the world-highest cut-off rigidity $P_c$. The average $P_m$ weighted by the count rate is 14.9 GeV for 20 NMs and 65.4 GV for 69 MDs. Therefore, there is a factor of 4.4 difference between the average $P_m$ monitored by these 20 NMs and 69 MDs. This motivates the present work to derive the rigidity spectrum of the GCR variation by analyzing NM and MD data altogether. Since $P_m$ of PSNM is 34.6 GV, at nearly half way between $P_m$ values monitored by 20 NMs and 69 MDs, PSNM data may play an important role in evaluating analyses of the rigidity dependence.

### 2.2 Analysis

We model the observed count rate, $I_{i,j}(t)$ in the $j$-th directional channel of the $i$-th detector, as

$$I_{i,j}^{fit}(t) = I_{i,j}^{CG}(t) + \sum_{n=0}^{2}\sum_{m=0}^{n}\{\xi_c^{n,m}(t)(c_{i,j}^{n,m}\cos m\omega t_i - s_{i,j}^{n,m}\sin m\omega t_i) + \xi_s^{n,m}(t)(s_{i,j}^{n,m}\cos m\omega t_i + c_{i,j}^{n,m}\sin m\omega t_i)\}, \quad (1)$$

where $\xi_c^{0,0}(t)$ is the cosmic ray density (or isotropic intensity), $\xi_c^{n,m}(t)$ and $\xi_s^{n,m}(t)$ for $1 \le n \le 2$, $0 \le m \le n$ are the components of cosmic ray anisotropy in the GEO coordinate system, $t_i$ is the local time in hour at the $i$-th detector, $c_{i,j}^{n,m}$ and $s_{i,j}^{n,m}$ are the coupling coefficients which relate

**Table 1: Characteristics of NMs and MDs**

| Station name | $P_c$(GV) | $P_m$(GV) |
|---|---|---|
| 20 NMs | | |
| APTY | 0.7 | 15.0 |
| ATHN | 8.5 | 22.8 |
| BKSN | 5.6 | 16.7 |
| CALM | 7.0 | 20.4 |
| DRBS | 3.2 | 15.5 |
| FSMT | 0.3 | 15.1 |
| INVK | 0.3 | 15.1 |
| IRK2 | 3.6 | 14.0 |
| KERG | 1.1 | 14.9 |
| LMKS | 3.8 | 13.5 |
| MXCO | 8.2 | 20.4 |
| NAIN | 0.3 | 15.1 |
| OULU | 0.8 | 14.9 |
| PWNK | 0.3 | 15.1 |
| SOPO | 0.1 | 11.3 |
| TERA | 0.0 | 14.8 |
| THUL | 0.3 | 15.0 |
| TXBY | 0.5 | 14.9 |
| PSNM | 16.7 | 34.6 |
| SYOW | 0.4 | 14.9 |
| 69 MD directional channels | | |
| Nagoya (17 directional channels) | 8.0-12.6 | 58.4-106.9 |
| Hobart (13 directional channels) | 2.5-4.0 | 53.1-74.0 |
| Kuwait (13 directional channels) | 8.9-14.1 | 61.2-104.0 |
| São Martinho (17 directional channels) | 7.1-14.1 | 54.3-98.4 |
| Syowa (9 directional channels) | 2.51-3.55 | 55.5-72.0 |

Note: $P_c$ and $P_m$ indicate the geomagnetic cut-off rigidity and the median rigidity of the detected primary GCRs, respectively.

(or "couple") the observed intensity in each directional channel with the cosmic ray density and anisotropy in space and $\omega = \pi/12$. In the GEO coordinate system, we set the $x$-axis to the anti-sunward direction in the equatorial plane, the $z$-axis to the geographical north perpendicular to the equatorial plane, and the $y$-axis completing the right-handed coordinate system. $I_{i,j}^{CG}(t)$ in Eq.(1) is a term representing the contribution to $I_{i,j}^{fit}(t)$ from the solar wind convection and the Compton-Getting anisotropy due to the Earth's orbital motion around Sun. The rigidity spectra $g_n(p,t)$ of the density and anisotropy are nessesary to caluclate $c_{i,j}^{n,m}$ and $s_{i,j}^{n,m}$. In this paper, we

assume the single power-law spectra, as

$$g_n(p,t) = \left(\frac{p}{p_r}\right)^{\gamma_n(t)}, \tag{2}$$

where $p$ is the rigidity of primary cosmic rays, $\gamma_n(t)$ is the power-law index and $p_r$ is the reference rigidity, which we set to be 15 GV and 65 GV as representative primary rigidities for NMs and MDs, respectively.

We calculate the amplitude of the first-order anisotropy ($A_1$) as

$$A_1 = \sqrt{\sum_{m=0}^{1}\{\xi_c^{1,m}(t)^2 + \xi_s^{1,m}(t)^2\}}, \tag{3}$$

Details of this analysis are provided in [4].

## 3. Results

The obtained best-fit parameters (GCR density, amplitude of the first-order anisotropy, and $\gamma_n$) are shown in Figure 3. Color shaded periods in this figure correspond to those in Figure 2.

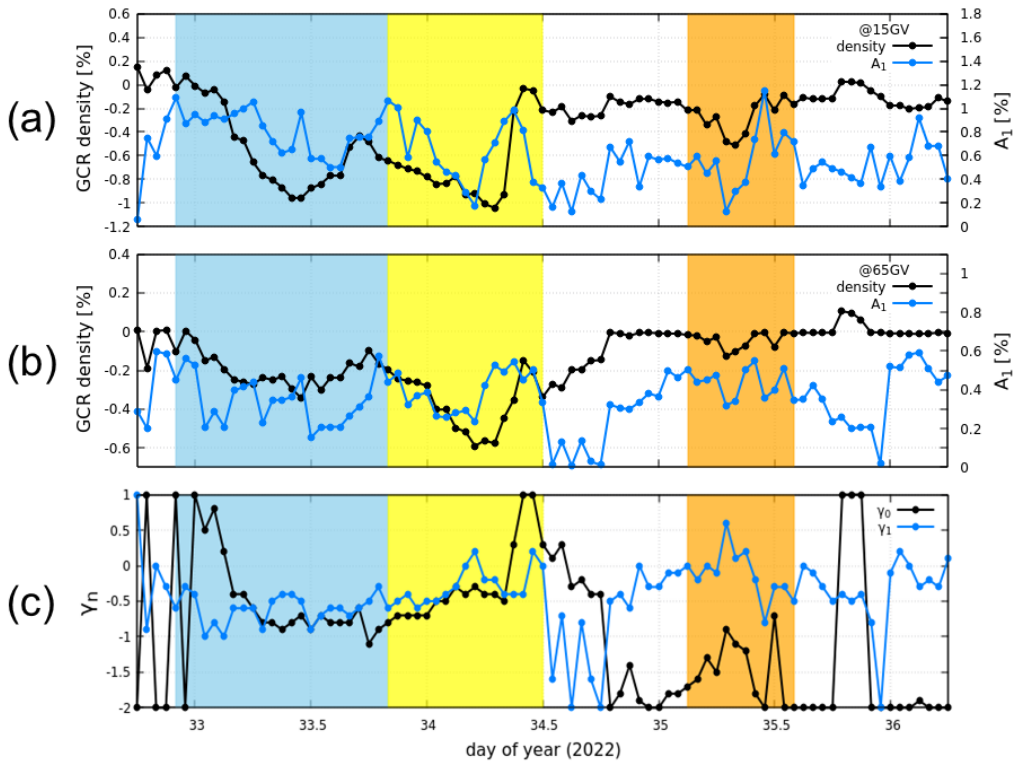


**Figure 3: Best-fit parameters obtained from NM and MD data.**
Panels (a) and (b) show the GCR density (black solid circles on the left vertical axes) and the amplitude of the first-order anisotropy $A_1$ (blue solid circles on the right vertical axes) at 15 GV and 65 GV, respectively. Bottom panel (c) shows the power-law index $\gamma_n$ ($n = 0$ for the cosmic ray density by black circles, $n = 1$ for the first-order anisotropy by blue circles). Color shaded periods in this figure correspond to those in Figure 2.

The GCR density shows a decrease at both 15 GV and 65 GV in all three periods. In the shock-sheath, the GCR density at 65 GV recovers to ~0% after the minimum, and then decreases again in FR1. On the other hand, the density at 15 GV recovers only to -0.4% in the shock-sheath before decreasing in FR1. The ratio of the maximum density decrease at 15 GV to that at 65GV in the shock-sheath is 3.4 indicating a spectrum with negative $\gamma_0$. The same ratio of maximum decreases in FR1 is 1.7 indicating a harder spectrum than in the shock-sheath.

The amplitude of the first-order anisotropy ($A_1$) at 65 GV is almost always smaller than that at 15 GV. $A_1$ at 15 GV exceeds 1% at the beginnings of the shock-sheath and FR1 and at the ending of FR1 and FR2. While similar variations are observed in $A_1$ at 15 GV in FR1 and FR2, there is no notable variation of $A_1$ at 65 GV seen in FR2.

In the shock-sheath, $\gamma_0$ decreases in the first half and remains almost constant in the second half. On the other hand, it remains almost constant in the first half and increases in the second half in FR1. In FR2, it increases and decreases in the first and second halves, respectively. $\gamma_0$ is uncertain before shock-sheath and after FR2 when the density variation is small. $\gamma_1$ is about 0 throughout the entire period except during 34.5 ~34.7 doy when $A_1$ is small.

## 4. Summary

On February 3, 2022, medium magnetic storms occurred and caused Starlink satellites' re-entry into the atmosphere (SpaceX. (2022)). In this paper, we analyzed NM network and GMDN data and deduced variations of the cosmic ray density and anisotropy during the event. Specifically, the cosmic ray density and anisotropy and their power-law spectral indices $\gamma_n$ were calculated every hour. In this "Starlink" event, the GCR density was decreasing in three periods, the shock-sheath, FR1, and FR2 periods. $\gamma_0$ and the amplitude of the first-order anisotropy ($A_1$) behaved similarly in FR1 and FR2 periods. These imply that large local magnetic structures existed suppressing GCR density inside FR1 and FR2 supporting the two flux ropes structure suggested by [1].

## 5. Acknowledgement

The Institute for Space-Earth Environmental Research (ISEE), Nagoya University, the Institute for Cosmic Ray Research (ICRR), University of Tokyo, and the "Strategic Research Projects" grant from ROIS (Research Organization of Information and Systems) in Japan. The observations are supported by Nagoya University with the Nagoya muon detector, by INPE and UFSM with the São Martinho da Serra muon detector, by the Australian Antarctic Division with the Hobart muon detector, and by project SP01/09 of the Research Administration of Kuwait University with the Kuwait City muon detector. N. J. S. thanks the Brazilian Agency- CNPq for the fellowship un- der grant number 300886/2016-0. EE would like to thank Brazilian funding agencies for research grants FAPESP (2018/21657-1) and CNPq (pQ-301883/2019-0). M. Rockenbach thanks the Brazil- ian Agency - CNPq for the fellowship under grant number 306995/2021-2. ADL thanks CNPq for grant 309916/2018-6. PSNM maintenance was also supported by Achara Seripienlert and the National Astronomical Research Institute of Thailand. We acknowledge the NMDB database (http://www.numdb.eu), founded under the European Union's FP7 program (contact no. 213007) for providing data. We also gratefully acknowledge the NOAA Air Resources Laboratory (ARL) for the

provision of GDAS data, which are available at the READY website (http://www.ready.noaa.gov) and used in this paper. The OMNIWeb dataset of the solar wind and IMF parameters is provided by the Goddard Space Flight Center, NASA, USA.

## References

[1] R. Kataoka et al., *Unexpected space weather causing the reentry of 38 Starlink satellites in February 2022*, J. Space Weather, 12, 41 (2022), http://doi.org/10.1051/swsc/2022034

[2] GMDN collaboration, Global Muon Detector Network (GMDN) data, http://hdl.handle.net/10091/0002001448

[3] R. R. S. Mendonça et al., *THE TEMPERATURE EFFECT IN SECONDARY COSMIC RAYS (MUONS) OBSERVED AT THE GROUND: ANALYSIS OF THE GLOBAL MUON DETECTOR NETWORK DATA*, Astrophys. J., 830 (2016), http://doi.org/10.3847/0004-637X/830/2/88

[4] K. Munakata et al., *Large amplitude bidirectional anisotropy of cosmic-ray intensity observed with world-wide networks of ground-based neutron monitors and muon detectors in November, 2021*, Astrophys. J., 938, 30 (2022), http://doi.org/10.3847/1538-4357/ac91c5

[5] W. Kihara et al., *A Peculiar ICME Event in August 2018 Observed With the Global Muon Detector Network*, J. Space Weather, 19, 3 (2021), http://doi.org/10.1029/2020SW002531

## Full Authors List: GMDN Collaboration

K. Munakata[1], M. Kozai[2], C. Kato[1], Y. Hayashi[1], Y. Masuda[1], R. Kataoka[3,4], A. Kadokura[2,3,4], S. Miyake[5], K. Iwai[6] R. R. S. Mendonça[7], E. Echer[7], A. Dal Lago[7], M. Rockenbach[7], N. J. Schuch[8], J. V. Bageston[8], C. R. Braga[9], H. K. Al Jassar[10], M. M. Sharma[10], M. L. Duldig[11], J. E. Humble[11], I. Sabbah[12], P.-S. Mangeard[13], T. Kuwabara[13], and P. Evenson[13]

[1]Department of Physics, Shinshu University, Matsumoto, Nagano 390-8621, Japan. [2]Polar Environment Data Science Center, Joint Support-Center for Data Science Research, Research Organization of Information and Systems, Tachikawa, Tokyo 190-0014, Japan. [3]National Institute of Polar Research, Tachikawa, Tokyo 190-8518, Japan. [4] Department of Polar Science, School of Multidisciplinary Sciences, The Graduate University for Advanced Studies, SOKENDAI, Tachikawa, Tokyo 190-8518, Japan. [5] National Institute of Technology (KOSEN), Ibaraki College, 866 Nakane, Hitachinaka-shi, Ibaraki-ken 312-8508 Japan. [6] Institute for Space-Earth Environmental Research, Nagoya University, Nagoya, Aichi 464-8601, Japan. [7] National Institute for Space Research (INPE), 12227-010 São José dos Campos, Brazil. [8] Southern Space Coordination, National Institute for Space Research, P.O. Box 5021-97110-970—Santa Maria, RS, Brazil. [9] George Mason University, 4400 University Drive, Fairfax, VA 22030, USA. [10] Physics Department, Kuwait University, P.O. Box 5969 Safat, 13060, Kuwait. [11] School of Natural Sciences, University of Tasmania, Hobart, Tasmania 7001, Australia. [12] Department of Laboratory Technology, College of Technological Studies, The Public Authority for Applied Education and Training, Shuwaikh, 72853, Kuwait. [13] Bartol Research Institute and Department of Physics and Astronomy, University of Delaware, 217 Sharp Laboratory, Newark, DE 19716, USA.

PoS(ICRC2023)1344